J Electr Eng Technol.2018; 13(1): 333-344
http://doi.org/10.5370/JEET.2018.13.1.333

ISSN(Print) 1975-0102
ISSN(Online) 2093-7423

An Optimization Design of the Diode Clamped Multi-Level Converter for Coaxial Inductive Power Transfer on the Low Voltage DC Micro-grid

Worapong Pairindra† and Surin Khomfoi*

Abstract – This proposed paper aims for the high efficiency contactless power transfer in household dc power distribution. A 300 W five-level diode clamped multi-level converter with 300 Vdc input dc link bus is employed for the power transferring task and the output voltage range is controlled at 48 Vdc. The inner and outer solenoid coils are used for inductive power transfer (IPT) transformer with the 200 kHz switching frequency for designed power density. Therefore, to achieve the converter efficiency above 95%, the LLC series resonant with fundamental harmonic analysis (FHA) and the calculated switching angles are used as an optimized tool for designing the system resonant tank. The validations of this approached topology are illustrated in both MATLAB/Simulink simulation and implementation.

Keywords: Diode clamped multi-level converter, LLC series resonant circuit, Inductive power transfer, Contactless transformer

1. Introduction

Nowadays, the renewable energy with various types of source generators has become more significant issues in power distribution system. In recent years, the smart-grid is introduced to the public with the advantages over the old fashion power distribution such as several types of distribution generator connected ability, two ways real time communication, controllable output power or improving the power system stability.

Generally, a single power unit of micro-grid can be operated in islanding mode or grid connected load operation with the combination of energy storages such as batteries or super capacitors, small generators or controllable loads. The micro-grid can be categorized into AC and DC link bus, dc micro-grid is a the next step of technology for domestic home power distribution which has many advantages [1] such as non synchronization process in order to deliver or receive the power over the micro-grid, non requirement for reactive power compensation and high efficiency power transfer due to the dc to dc power conversion. However, the major penalty for dc micro-grid can be expressed in terms of initial cost for new infrastructure, protection and adapted voltage variation loads in dc power distribution.

From previous discussion, the household power distribution is in public focus, according to the emergence of the renewable sources such as photovoltaic, wind or fuel cell energy, the multiple renewable sources will be integrated and obtained the high efficiency for household power distribution with the dc micro-grid. The power electronics converter with high power density has become a major challenge for many researchers. The direct current household power distribution is one of the promising futures for the next generation to transfer the renewable power sources directly to the load. However, the direct metal contact power transfer such as conventional plug and receptacle is a major consequence for dc power distribution. Therefore, the high frequency converter with inductive power transfer (IPT) is introduced in this proposed paper in order to overcome the problems such as the risk of electric shock, arch discharge and galvanic isolation.

The inductive power transferring technology [2-6] is based on energy transfer over the magnetic field from primary coil to the pickup side at secondary coil. The new concept design of contactless power transfer [7-9] is illustrated in Fig. 1(a). The separable transformer with air core functions as a power transfer unit and connected to the high frequency power converter. The transformer consists of two solenoid coils as shown in Fig. 1(b). The inner coil can be described as a secondary coil of the

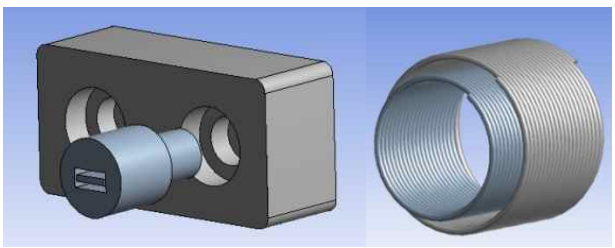

(a) (b)

Fig. 1. Coaxial contactless transformer ideal concept design

† Corresponding Author: Dept. of Electrical Engineering, Faculty of Engineering, King Mongkut's Institute of Technology Ladkrabang, Thailand. (worapong73@hotmail.com)
* Dept. of Electrical Engineering, Faculty of Engineering, King Mongkut's Institute of Technology Ladkrabang, Thailand. (kkhsurin@kmitl.ac.th)
Received: November 6, 2016 ; Accepted: October 21, 2017

contactless transformer and the outer shelter coil is connected to the high frequency converter. Therefore, there is no physical contact between the two coils and high frequency power converter creates a strong electromagnetic coupling in order to link or send power to the secondary side. However, the coaxial contactless transformer design with square wave input voltage such as conventional half-bridge or full-bridge converter has less power density than the sinusoid wave form converter. Therefore, the multi-level converter is introduced [10] in this proposed paper to enhance the power density of overall system. The common issues of designing the power converter are the high efficiency, high power density and cost effectiveness. Recently, the resonant power converter has become more attractive in power converter design, especially the LLC series resonant configuration has higher switching ability with lower losses in switching devices.

In summary, this proposed paper is dealing with the enhancement of IPT system by adding the designed resonance circuit for soft switching topology, the diode clamped multi-level converter (DCML) has been chosen to deliver high frequency with low THD through the contactless solenoid core transformer, and generates strong electromagnetic coupling in order to operate at 300 W at the converter rear side. The proposed paper is categorized as follows, In section 2, an overall structure and principle analysis of DCML with arrangement of inductive power transfer and LLC series resonant circuit is described. The multi-level converter is clarified in section 3. Subsequently, the simulation and experimental results are shown in section 4 and 5 with the summary in section 6, respectively.

2. Structure and Principle Analysis of DCML with Resonant IPT

Fig. 2. shows the structure of the DCML power converter connected to the resonant tank with IPT contactless transformer. A 300 V direct current input bus connects to the DCML as a common dc link bus source, and powers the contactless transformer. In order to achieve the high efficiency converter, the resonant tank is designed with the passive elements such as capacitor, inductor and reflects impedance to operate as a resonant converter. Theoretically, the DCML with higher level or more switching device pairs will improve the power quality of the system which leads to the optimized design for the contactless transformer. Therefore, a five-level DCML has been introduced to enhance the power density of the converter due to the sinusoid wave form calculation. At the rear side, the output regulated voltage is controlled and varied by the frequency control algorithm with the discrete controller.

2.1. LLC series resonant structure

The LLC series resonant with half-bridge converter has been described in [11, 12]. The simplifier circuit for the voltage gain which is a ratio between the output against the input voltage is shown in Fig. 3. Hence, the design procedure of the resonant tank parameters depends on the calculation of this typical voltage gain model and input parameter specifications. The practical design with the traditional methods such as state plan or time-domain [12] analysis has many difficulties in precision of math model equation which cannot be accurately written. In order to solve the mathematical equation for the system voltage gain, the fundamental harmonic approximation has been introduced in this proposed paper for sinusoidal voltage and current wave form analysis.

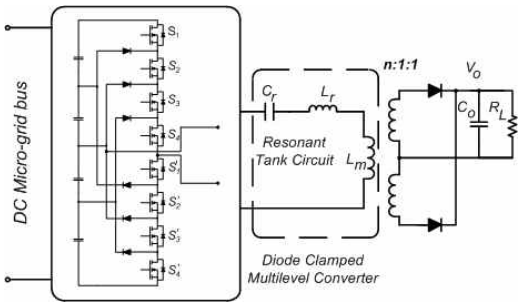

Fig. 2. The structure of DCML with IPT schematic

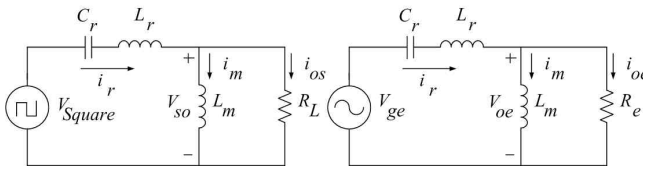

Fig. 3. (a) Simplified system circuit (b) Linear sinusoid circuit

In Fig. 3, the relationship of the simplified fundamental input voltage (V_{ge}) variables of staircase signal can be described as follows:

$$V_{ge}(t) = \frac{4}{\pi} \cdot V_{max} \cdot \sin\left(2\pi f_{sw} t\right) \tag{1}$$

The RMS value is

$$\mathrm{V_{ge\_rms}} = \frac{\sqrt{2}}{\pi} \cdot V_{DC} \tag{2}$$

The fundamental output voltage of the staircase signal can be written as follows:

$$V_{oe}(t) = \frac{4}{\pi} \cdot n \cdot V_{out} \cdot \sin\left(2\pi f_{sw} t - \varphi_v\right) \tag{3}$$

The φ_v is an angle between input and output voltage, with RMS value

$$V_{oe\_rms} = \frac{2\sqrt{2}}{\pi} \cdot n \cdot V_{out} \tag{4}$$

The fundamental output current can be found

$$i_{oe}(t) = \frac{\pi}{2} \cdot \frac{1}{n} \cdot I_{out} \cdot \sin(2\pi f_{sw} t - \varphi_i) \tag{5}$$

The φ_i is an angle between i_{oe} and V_{oe}, and the current RMS value is

$$I_{oe\_rms} = \frac{\pi}{2\sqrt{2}} \cdot \frac{1}{n} \cdot I_{out} \tag{6}$$

Equivalent load resistor, R_e can be calculated as follows:

$$R_e = \frac{V_{oe}}{I_{oe}} = \frac{8 \times n^2}{\pi^2} \times \frac{V_{out}}{I_{out}} = \frac{8 \times n^2}{\pi^2} \times R_L \tag{7}$$

After investigating in equation above, the equivalent resistance depends on the turn ratio and the load resistive due to the sinusoidal wave form calculation, the angular frequency is

$$\omega = \omega_{sw} = 2\pi f_{sw} \tag{8}$$

The resonant capacitor, resonant inductor and magnetized inductor can be described as

$$X_{Cr} = \frac{1}{\omega C_r}, X_{Lr} = \omega L_r, X_{Lm} = \omega L_m \tag{9}$$

The RMS magnetized current is

$$I_m = \frac{V_{oe}}{\omega L_m} = \frac{2\sqrt{2}}{\pi} \times \frac{n \times V_{out}}{\omega L_m} \tag{10}$$

and the total resonant current, I_r

$$I_r = \sqrt{I_m^2 + I_{oe}^2} \tag{11}$$

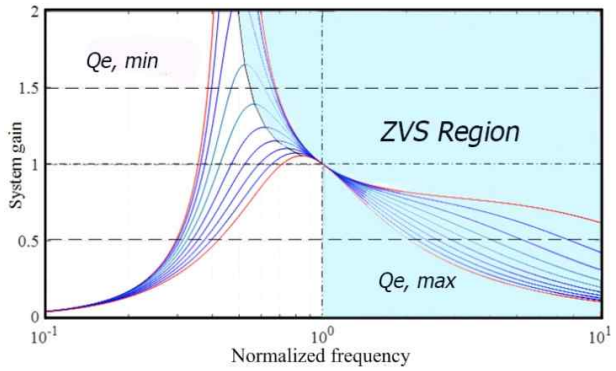

Fig. 4. Voltage gain vs nomalized frequency

Fig. 4 shows the relationship of the output voltage gain in the LLC series resonant and the frequency can be expressed as

$$M_g = \frac{V_{oe}}{V_{ge}} = \left| \frac{jX_{Lm} // R_e}{(jX_{Lm} // R_e) + j(X_{Lr} - X_{Cr})} \right| \tag{12}$$

Rewritten at the new form

$$M_g = \left| \frac{L_n \times f_n^2}{\left[(L_n + 1) \times f_n^2 - 1\right] + j\left[\left(f_n^2 - 1\right) \times f_n \times Q_e \times L_n\right]} \right| \tag{13}$$

Which

f_n	Normalized frequency	L_n	Inductor ratio
f_{sw}	Switching frequency	f_o	Resonant frequency
L_r	Resonant inductor	L_m	Magnetized inductor
C_r	Resonant capacitor	R_e	Equivalent resistor

Normalized frequency equal is expressed as

$$f_n = \frac{f_{sw}}{f_o} \tag{14}$$

Inductor ratio can be defined as

$$L_n = \frac{L_m}{L_r} \tag{15}$$

Quality factor of the resonant converter can be described

$$Q_e = \frac{\sqrt{L_r / C_r}}{R_e} \tag{16}$$

2.2. Boundary design procedure

The design consideration for the resonant converter is the frequency modulation. The regulated output voltage can be modified by the normalized frequency, the system maximum and minimum frequency to be operated depends on the calculated maximum and minimum gain from the given input parameters as shown in the following equation and can be plotted in various load fluctuations in Fig. 5.

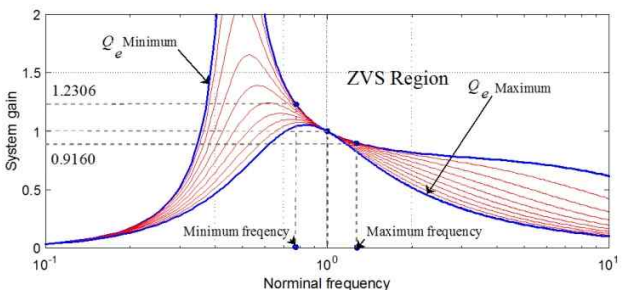

Fig. 5. Operation boundary design

Table 1. LLC Series resonant system gain design

Component	Parameter
Nominal frequency	200 kHz
Maximum frequency	240 kHz
Minimum frequency	154 kHz
Maximum gain	1.2306
Minimum gain	0.9160

$$M_{g\_max} = \frac{n \times V_{0\_max}}{\frac{V_{in\_min}}{2}} \quad (17)$$

$$M_{g\_min} = \frac{n \times V_{0\_min}}{\frac{V_{in\_max}}{2}} \quad (18)$$

3. Multi-level Converter

3.1. Multi-level converter overview

The concept of the multi-level converter [13, 14] for power electronics applications in dc low voltage power distribution has been introduced in this proposed paper. The synthesized stair case voltage is obtained by using the series connecting the power semiconductor devices with the isolated low voltage dc power sources. For example, the capacitors, batteries, renewable sources can be used as a multiple dc power source. The multi-level converter has many advantages due to wave form quality, common mode voltage, low input current distortion and operating in both fundamental switching frequency and high switching frequency. Nevertheless, the multi-level converter main disadvantage with the numbers of switching devices is still being investigated by many researchers concerning the converter complexity and cost relativity.

Recently, there are many types of multi-level converters that have been introduced for power conversion: the cascaded H-bridge with isolated dc power source, diode clamped and flying capacitors. Many modulation techniques and control algorithms for multi-level converter enhancement such as sinusoidal pulse width (SPWM) and selective harmonic elimination (SHE-PWM), space vector modulation (SVM) have been introduced during the last two decades.

Generally, the high power density design of the contactless transformer system requires a low THD input voltage wave form. In order to achieve the objective, the diode clamped multi-level converter has been chosen for generating the five-level stair case wave form, due to advantages of using direct common input dc power source with high switching frequency compares with SPWM and less expensive than flying capacitor converter. Table 2 illustrates the switching state of the diode clamped DCML topology. The contactless primary coil receives direct power from the five-level diode clamped converter as shown in Fig. 6 with the control algorithm in Fig. 7.

Table 2. Diode clamped multi-level switching state

V_{out}	Switching state							
	S_1	S_2	S_3	S_4	S_1'	S_2'	S_3'	S_4'
150 V	1	1	1	1	0	0	0	0
75 V	0	1	1	1	1	0	0	0
0 V	0	0	1	1	1	1	0	0
-75 V	0	0	0	1	1	1	1	0
-150 V	0	0	0	0	1	1	1	1

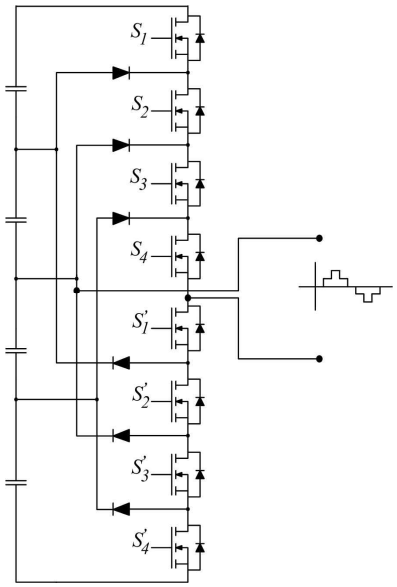

Fig. 6. The five-level diode clamped mutilevel converter scheme

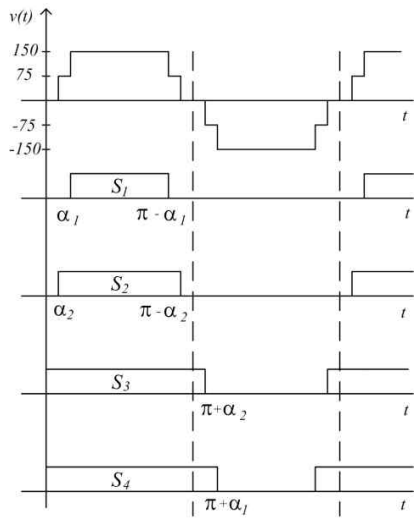

Fig. 7. Upper portion switching toplogy

3.2. Selective harmonics elimination

The first priority design for the optimization with IPT system deals with the power density as mentioned in the previous section. Therefore, the fundamental switching with the selective harmonic elimination has been chosen

for this optimied outcome voltage. Fig. 8 shows the angle in each level, the magnitude of the fundamental harmonic and the order of the harmonic can be determined with the concurrent changing angles.

From Fig. 7, the output of the synthesized staircase voltage can be explained using a polynomial equation, and can be solved in the elimination equation method. The Fourier equation for bipolar square wave is applied and can be expressed as following equation.

Odd value

$$V_{out,n} = \frac{4}{n\pi}\left[V_{DC}\cos(n\alpha_1) + V_{DC}\cos(n\alpha_2) + \ldots + V_{DC}\cos(n\alpha_{(L-1)/2})\right] \quad (19)$$

Where n is the harmonic order and V_{DC} is a voltage for each level of DCML converter, generally, by changing the proper angles of each level, the low frequency harmonics can be eliminated from the output. Therefore, selective harmonic elimination (SHE) is introduced for harmonic elimination. For example, the third harmonic is chosen to be removed. The form of the equation can be described from previous equation as follows:

Fundamental output equation

$$V_{out,1} = \frac{4V_{DC}}{\pi}\left[\cos(\alpha_1) + \cos(\alpha_2)\right] \quad (20)$$

3rd harmonic output equation

$$V_{out,3} = \frac{4V_{DC}}{3\pi}\left[\cos(3\alpha_1) + \cos(3\alpha_2)\right] \quad (21)$$

In the modulation index, M_A is a ratio between $4V_{DC}/\pi$ and $V_{out,1}$. With the proper angles, the third harmonic should be removed from the output of the DCML and the fundamental harmonic can be controlled at the desired level as well.

The non linear polynomial equations are solved with Newton Raphson's method, and the third harmonic elimination switching angles are calculated from polynomial equations as shown in following equations;

$$\cos(1\alpha_1) + \cos(1\alpha_2) = \frac{\pi}{4V_{DC}}V_{out,1} = M_A \quad (22)$$

$$\cos(3\alpha_1) + \cos(3\alpha_2) = 0 \quad (23)$$

where

$$\cos(3\alpha) = 4\cos^3\alpha - 3\cos\alpha \quad (24)$$

$$4\cos^3(\alpha_1) - 3\cos(\alpha_1) + 4\cos^3(\alpha_2) - 3\cos(\alpha_2) = 0 \quad (25)$$

The pair of sets of the switching angles are illustrated in Fig. 8. in terms of two switching angles curves versus the modulation index. From this point, the unnecessary voltage harmonic will be disappeared and the fundamental amplitude output voltage can be approximately setup at satisfied level.

3.3. The LLC series resonant with DCML operation mode

The LLC series resonant circuit is applied to the rear side of the DCML for operating in frequency control converter and operates in different kinds of modes depending on the switching states. Each operating mode has individual set of PWM for the controller. Initially, the TI TMS320F28335 microcontroller generates 4 non-inverting and 4 inverting controlled signals, the switching frequency and dead band are also integrated in MATLAB/ Simulink C2000 block set which are set at 5 μ S and 0.03 μ S (approximately 1%), respectively. To prevent the shoot through current, the dead time has been deployed for avoiding the short circuit from DC positive terminal directly to the negative side. However, the dead band should be limited in appropriate length to keep the output at a desirable voltage waveform. For example, the long

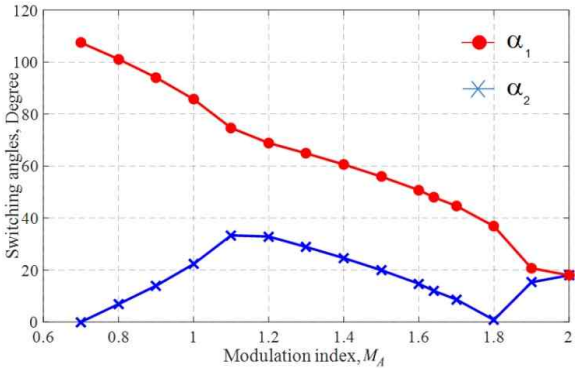

Fig. 8. Switching angles vs modulation index

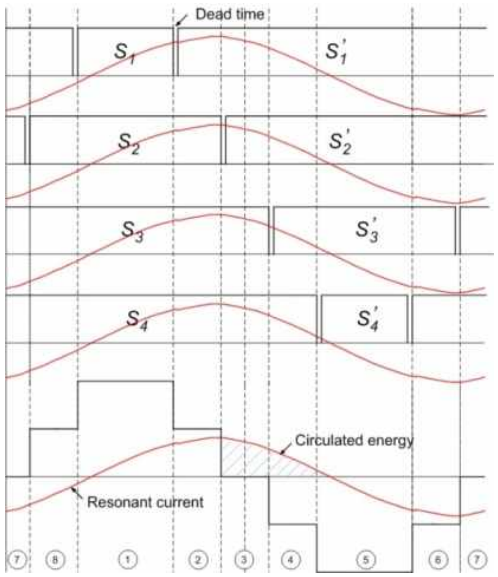

Fig. 9. Operation mode of DCML and resonant circuit

dead time may force the MOSFET 1 and MOSFET 4' to turn OFF in a period of time during the ON state interrupting the continuality current and lose the ability of ZVS condition. The operation mode can be described as follows:

Fig. 9. illustrades the switching topology of the diode clamped multi-level converter with the resonant tank circuit. The secondary reflected impedance can be described as.

$$Z_{Reflect} = \frac{\omega^2 M^2}{Z_L + j\omega L_S} \quad (26)$$

The primary current is shifted in order to achieved the soft switching condition and can be derived in difference operating modes as follows;

Operation mode 1 : The upper portion (S_1, S_2, S_3 and S_4) switches are turned on and supplied by V_{DC1} and V_{DC2}. D_1, D_2, D_3 perform as blocking diodes. The inverter output is set at V_{DC1}+V_{DC2}. Due to the reversing current direction, the circulating energy from the resonant tank provides the negative current through the body diode of S_1, S_2, S_3 and S_4 as shown in Fig. 10. and Fig. 11.

Operation mode 2 : The S_1 is turned off, the forward bias current starts to flow through the D_1, S_2, S_3 and S_4 and powered by only V_{DC2}. The output voltage is matched to the source voltage at V_{DC2}. Likewise, the resonant current will consist on the source current and the traped energy current as shown in Fig. 12.

Operation mode 3 : S_1 and S_2 are turned off, there is no current from sources to the output. However, there is still remaining energy in the resonant tank to force the current in the positive direction as illutrated in Fig. 13.

Operation mode 4 : Switch S_4,S'_1,S'_2 and S'_3 are turned on, D_3 is in forward bias condition. The negtive voltage of V_{DC3} will appear at the end of the inverter with -V_{DC3} level. The schematic is shown in Fig. 14.

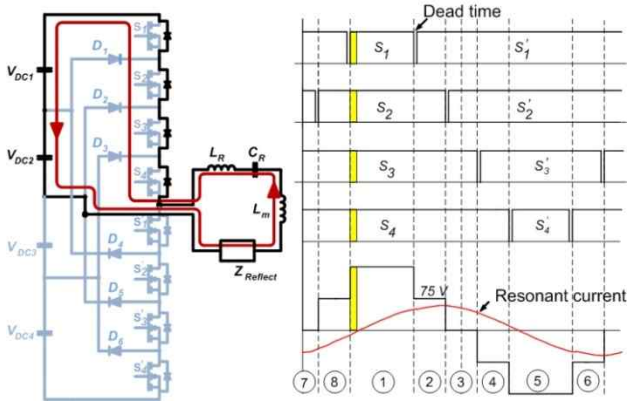

Fig. 10. Operation mode 1(Negative current)

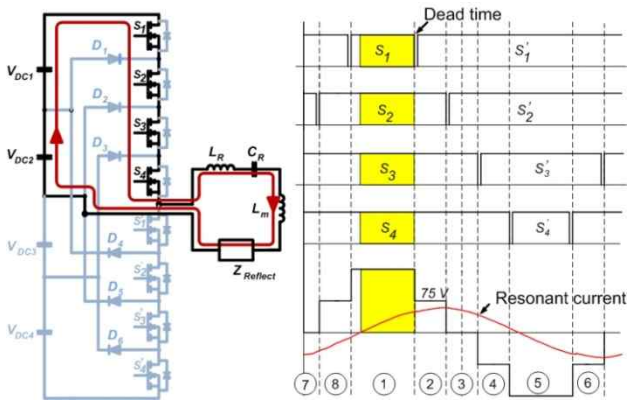

Fig. 11. Operation mode 1(Positive current)

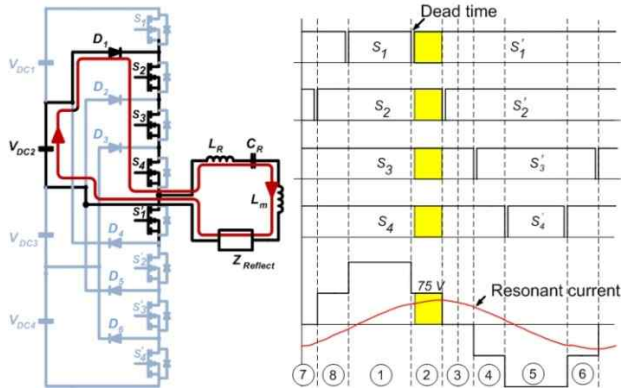

Fig. 12. Operation mode 2

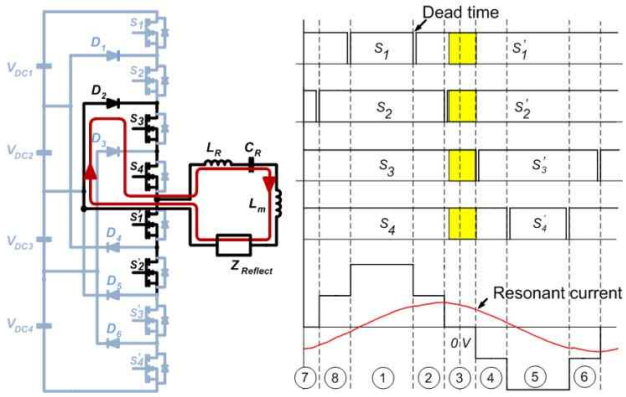

Fig. 13. Operation mode 3

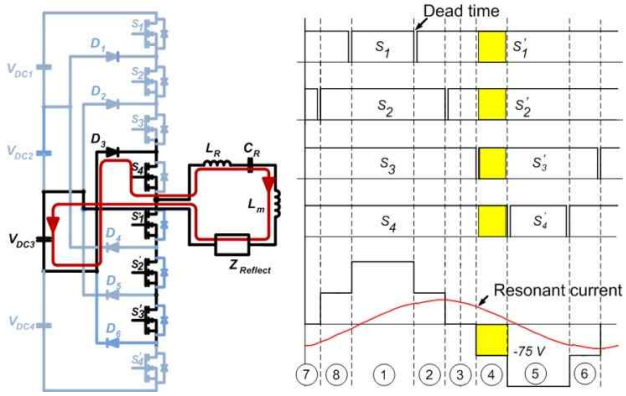

Fig. 14. Operation mode 4

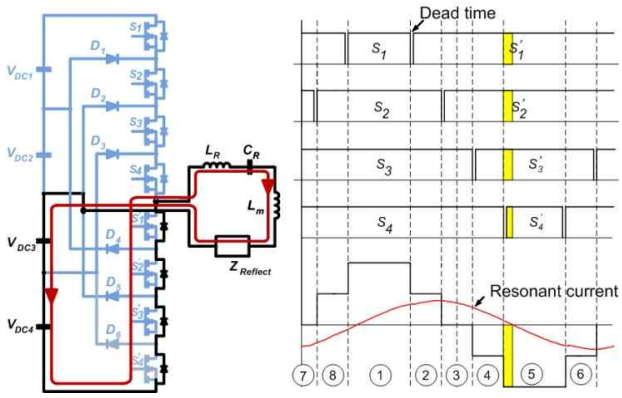

Fig. 15. Operation mode 5 (Positive current)

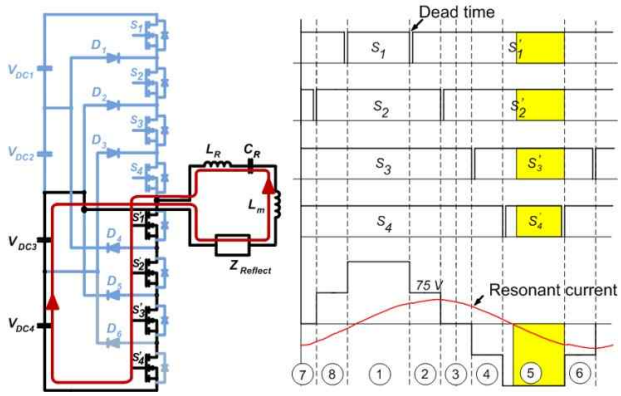

Fig. 16. Operation mode 5 (Negative current)

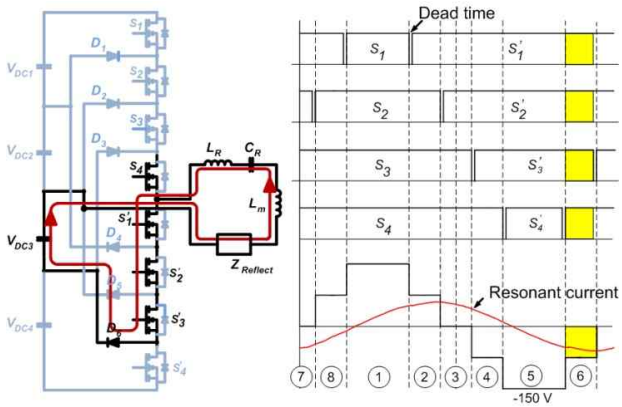

Fig. 17. Operation mode 6

Operation mode 5 : The Lower portion (S'_1, S'_2, S'_3 and S'_4) switches are turned on and supplied by V_{DC3} and V_{DC4}. D_4, D_5, D_6 perform as blocking diodes. The inverter output is set at V_{DC3}+V_{DC4}. Due to the reversing current direction, the circulating energy from the resonant tank provides the negative current through the body diode of S'_1, S'_2, S'_3 and S'_4 as shown in Fig. 15 and Fig. 16.

Operation mode 6 : S'_4 is turned off, the forward bias current starts to flow through D_6, S'_1, S'_2, and S'_3 are powered by only V_{DC3}, the output voltage is matched to the source voltage at V_{DC3}. Likewise, the resonant current will consist on the source current and the traped energy current as shown in Fig. 17.

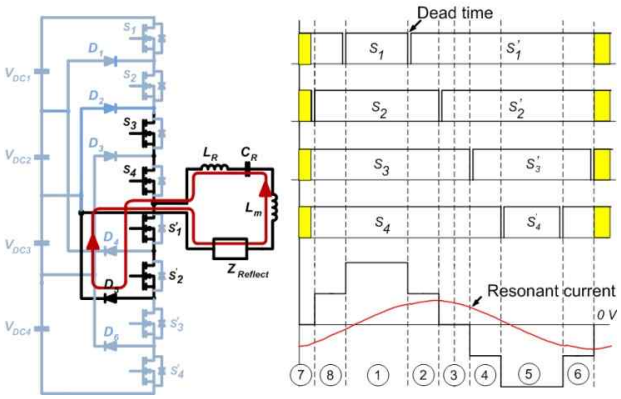

Fig. 18. Operation mode 7

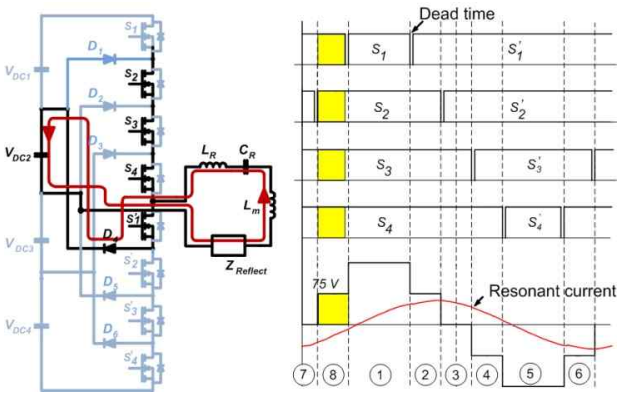

Fig. 19. Operation mode 8

Operation mode 7 : S'_3 and S'_4 are turned off, there is no current from sources to the output. However, there is still remaining energy in the resonant tank to force the current in the negative direction as illutrated in Fig. 18.

Operation mode 8 : Switch S'_3, S_4, $S'_1$and S'_2 are turned on. D_4 is in forward bias condition. The positive voltage of V_{DC2} will appeare at the end of the inverter with V_{DC2} level. The schematic is shown in Fig. 19.

The L_m is designed and calculated at a fixed value by using the fundamental harmonic analysis (FHA) technique which has the relationship between resonant inductor and resonant capacitor at the precise specification (rated power, switching frequency, etc). According to the FHA calculation, the relationship of the L_m, L_r and C_r can be described in equation (27)-(29), which can be seen in [12] for designed procedures.

$$C_r = \frac{1}{2\pi f_{SW} R_e Q_e} \tag{27}$$

$$L_r = \frac{1}{\left(2\pi f_{SW}\right)^2 C_r} \tag{28}$$

$$L_m = L_n \times L_r \tag{29}$$

During the light load condition may cause the resonant current to shift away from the designed point. However, the system gain can be maintained at the same value of the approximately normalized frequency and the zero voltage switching condition can still be achieved (ZVS condition in light blue zone of Fig. 4) under the situation in both mode 3 and 4. Additionally, the resonant current in mode 5 drops to negative because the energy released from an inductor at this state, in the resonant tank is much greater than the energy from the capacitor source, therefore, the resonant current will be starting to flow in a negative direction.

4. Simulation Results

Initially, the proposed method was simulated and validated with the MATLAB/Simulink. The system designed parameters are shown in Table 3 to 5 as same as the experimental setup. The %THD of DCML with the proper angles for the third and fifth harmonic elimination are illustrated in Fig. 20. It is found that, the optimized angles for five-level with modulation index 1.64 are 12 degree and 48 degree, respectively.

The resonant tank is connected at the end of DCML and performed resonant circuitry. Fig. 21. and Fig. 22. illustrate the magnitude (% of fundamental) simulation results of the input voltage of the contactless transformer. It could be noticed that without the auxiliary switching circuit circuitry, the resonant tank circuit was able to perform soft switching with ZVS condition. Fig. 23.-26. show the voltage and current shifted signals of the upper portion of each MOSFET switching device.

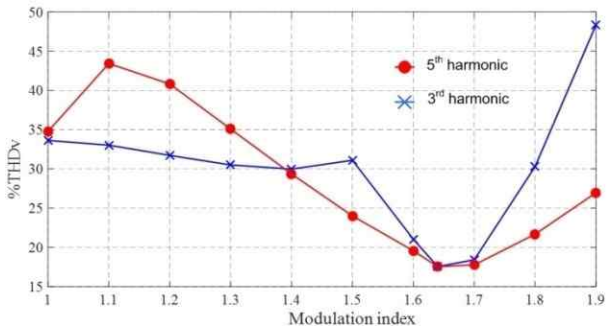

Fig. 20. The SHE %THD vs modulation index

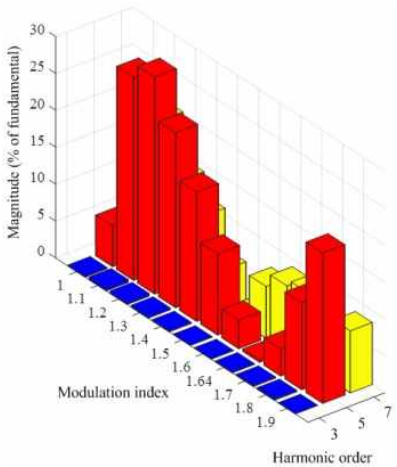

Fig. 21. 3rd harmonic elimination vs modulation index

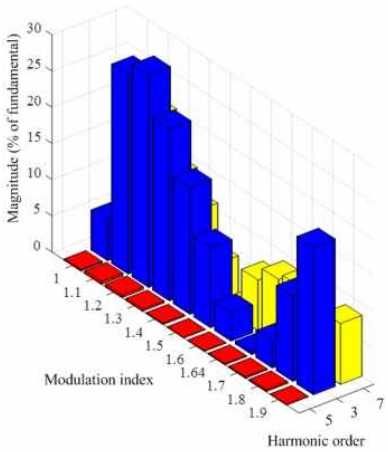

Fig. 22. 5th harmonic elimination vs modulation index

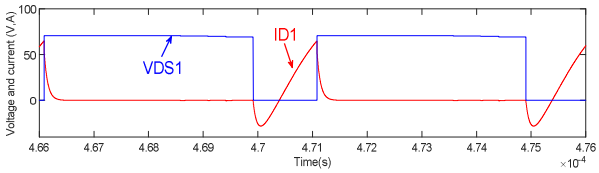

Fig. 23. V_{DS1} vs S_1 current

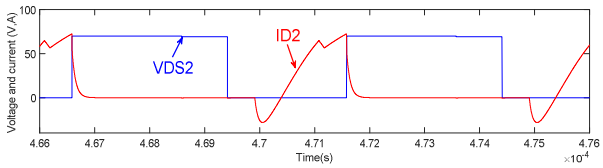

Fig. 24. V_{DS2} vs S_2 current

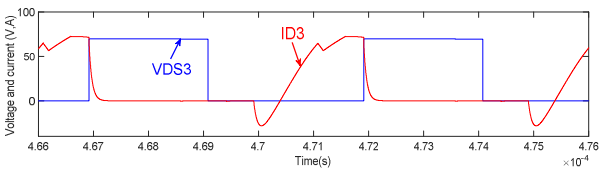

Fig. 25. V_{DS3} vs S_3 current

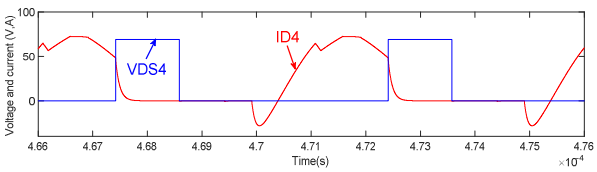

Fig. 26. V_{DS4} vs S_4 current

5. Experimental Results

The prototype converter has been built for testing and evaluation. A 300 W diode clamped multi-level converter with the optimized angles generates five-level output voltage for the contactless transformer and sends the power through the air core with the high frequency switching. The designed parameters of a 300 V input dc link bus voltage and electric home appliances output voltage are set at 48 V with 200 kHz switching frequency are shown in Table 3. To achieve the high efficiency converter target, the resonant circuit is needed to attach to the rear side of the DCML for shifting the switching current and voltage which are illustrated in Table 4 Table 5 shows the designed specification parameters of the contactless transformer. The primary inductance of the solenoid coil is designed to suit the resonant condition with the ability to transfer 300W power without the ferrite core.

Table 3. Specification of the prototype converter

Prototype specification	Parameter
Input DC link voltage	300 V
Output voltage	48 V
Switching frequency	200 kHz

Table 4. Diode clamped multi-level converter components

Component	Parameter
Resonant inductor	23.24 μH
Resonant capacitor	27.24 nF
Magnetized inductor	81.36 μH
Switching device	IRF740
High speed diode	MUR840
High speed driver	FOD3184

Table 5. Contactless transformer specification

Wire type	SWG 17	SWG 12
Turns	57	30
Layer per turn	1	1
Diameter	≈ 65 mm	≈ 60 mm
High	≈ 80 mm	≈ 80 mm

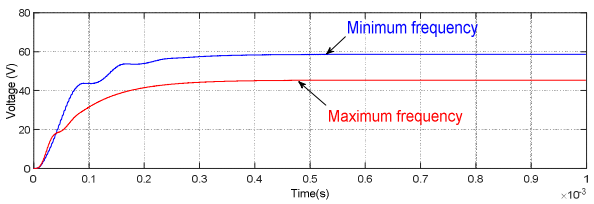

Fig. 27. Switching gain boundary

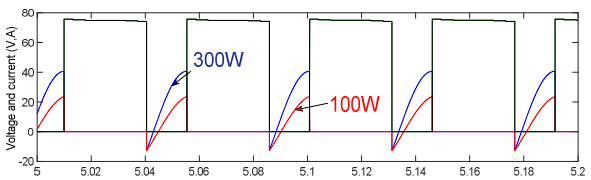

Fig. 28. V_{DS1} and current at 100 W and 300W

The five-level power converter is powered by the dc link bus voltage and controlled by the pulse width modulation signal. Previous sections show that, the optimized angle of the power converter can be calculated with the selective harmonic elimination (SHE) technique. After applying the system configuration in Table 3 to 5, the output voltage of the DCML with resonant tank performs ZVS condition under the load variation as shown in Fig. 36.

Apparently, each switching device operates in the ZVS

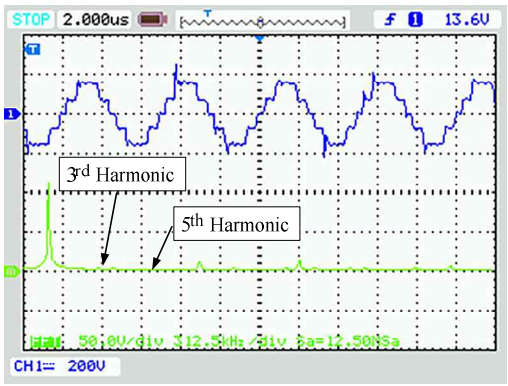

Fig. 29. The DCML output voltage and voltage harmonic spectrum *(CH I 200 V/DIV, FFT 50.0V/DIV, 312.5 kHz/DIV, Sa 12.5 NSa)*

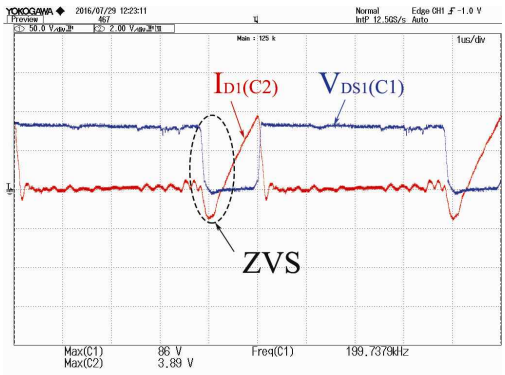

Fig. 30. V_{DS1} and current of S_1 (I_{D1} *2A/DIV*, V_{DS1} *50V/DIV)*

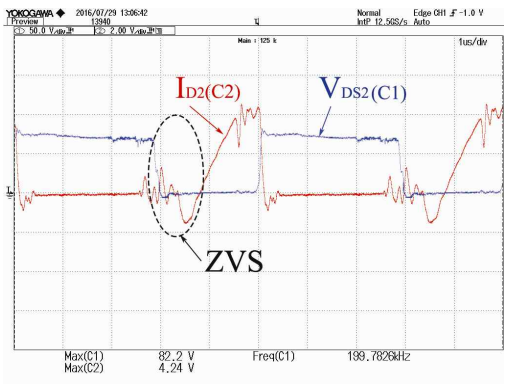

Fig. 31. V_{DS2} and current of S_2 (I_{D2} *2A/DIV*, V_{DS2} *50V/DIV)*

condition, for example, the upper portion signal can be seen from Fig. 30 to Fig. 33 and power dispatched in each power switched can be calculated or measured with the oscilloscope in average of multiplying mode between current and voltage. The total power loss of switching devices in DCML with contactless power transfer is 10.8W (3.6%) from total of 300 W input power. Fig. 35 shows the sector numbers from 1 to 8 which represents the power losses in the switching devices from S_1 to S_4', respectively.

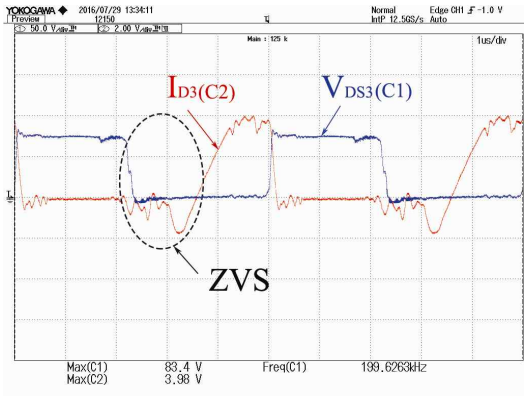

Fig. 32. V_{DS3} and current of S_3 (I_{D3} *2A/DIV*, V_{DS3} *50V/DIV)*

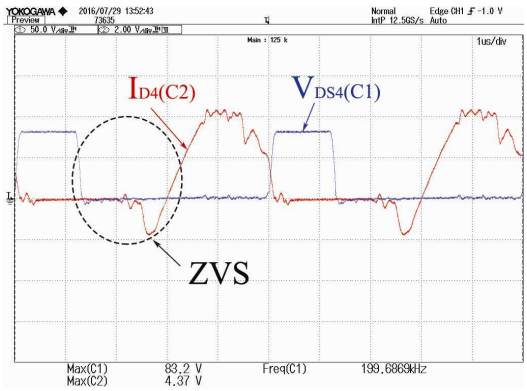

Fig. 33. V_{DS4} and current of S_4 (I_{D4} *2A/DIV*, V_{DS4} *50V/DIV)*

The contactless power transfer with coupling coefficient, k, is measured from total mutual coupling of the solenoid transformer coils, and the maximum efficiency of the transformer is 83.8% at 150 W for a single layer solenoid with the coupling coefficient, k equals to 0.91. In addition, the output voltage is controlled by varying the frequency in the specific boundary range according to designed maximum and minimum values of the system gain.

The proposed SHE technique is used for the switching algorithm in this research. The air core voltage harmonic spectrum is illustrated in Fig. 29. Obviously, the third and fifth harmonic orders with 200-kHz fundamental harmonic are almost eliminated from the total contents, and the THD_V is approximately equal to 17%.

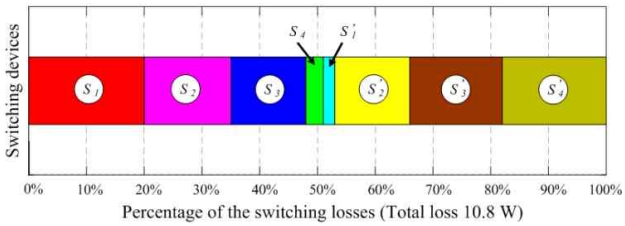

Fig. 35. Switching losses in DCML swtiching devices

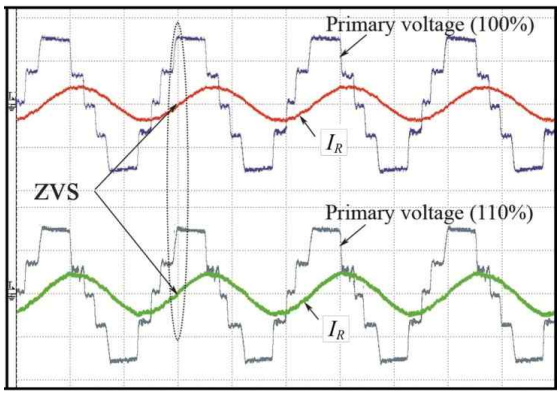

Fig. 36. The DCML ZVS under load variation (I_r *10A/DIV*, $V_{primary}$ *100V/DIV, T 2 µS/DIV)*

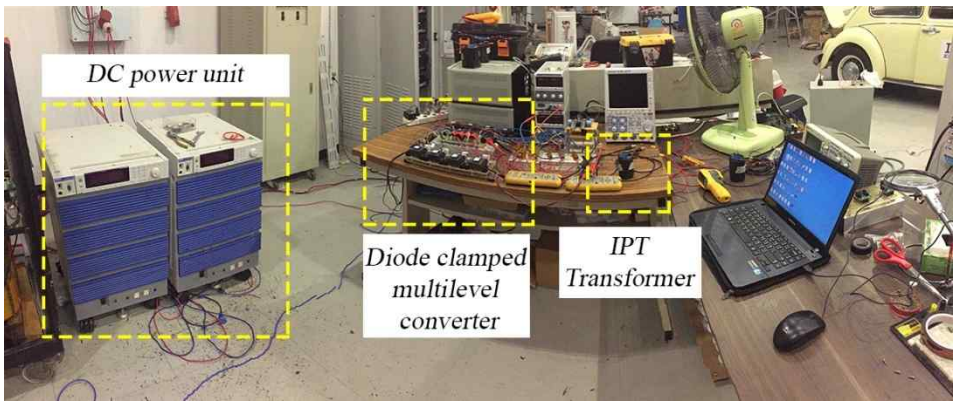

Fig. 34. Prototype experimental setup

6. Conclusion

The prototype of a contactless transformer with DCML was implemented in the terms of the calculated parameters substitution. The MATLAB/Simulink simulation program functioned as a simulator, in order to investigate the behavior of the overall system. Eventually, the outcome of the soft switching (ZVS) perfectly performed phase shifted between V_{DS} and the primary current in wide range of the load variation. The cost effectiveness has become a main idea for the proposed paper. Without adding the auxiliary switching circuit to DCML, the passive elements play the important role to perform the ZVS for DCML switching devices. Additional, the DCML with higher switching frequency will dramatically reduce the size of the IPT and increase the system power density as well. Finally, the inductive power transfer has proved that, the next step of the high efficiency dc low voltage distribution can be applied to household electric appliances with direct connected renewable sources in the near future.

References

[1] Ambarnath Banerji, DebasmitaSen, Ayan, K. Bera, Debtanu Ray, Debjyoti Paul, Anurag Bhakat, Sujit K. Biswas "MICROGRID : A Review," *Proceedings of IEEE GHTC-SAS* (*2013*), Thiruvananthapuram Trivandrum, India, Aug. 2013.

[2] P. Worapong, K. Surin, "The Optimization of Series Resonant LLC Half-Bridge Converter with Coreless Transformer Design in a Low Voltage DC Distribution System," *in Proceedings of IEEE ECTI-CON 2015*, Hua Hin, Thailand, June 2015.

[3] P. Worapong, K. Surin, "The Enhancement of Multi-level Converter for Coaxial Inductive Power Transfer in Low Voltage DC Power Distribution," *in Proceedings of IEEE ECTI-CON 2016*, Chiangmai, Thailand, June 2016.

[4] P. Worapong, K. Surin, "Development of a Cascaded Half-Bridge Converter with Contactless Transformer in DC Microgrid," *Elsevier publishing, Procedia Computer Science*, vol. 86, pp. 317-320, 2016.

[5] Sangwook Han, and David D. Wentzloff, "Wireless Power Transfer Using Resonant Inductive Coupling for 3D Integrated ICs," *in Proceedings of IEEE 3D Systems Integration Conference (3DIC) 2010*, Munich, Germany, Nov. 2010.

[6] Xiao Lu, Ping Wang, Dusit Niyato, Dong In Kim and Zhu Han, "Wireless Charging Technologies: Fundamentals, Standards, and Network Applications," *IEEE Trans. Wireless Communications*, vol. 22, no. 2, pp. 126-135, April 2015.

[7] Yushi Miiura, Satoshi Ojika, Tomofumi Ise, "Voltage Control of Inductive Contactless Power Transfer System with Coaxial Coreless Transformer for DC Power Distribution," *in Proceedings of IEEE IPEC 2014,* Hiroshima, Japan, pp. 1430-1437, May 2014.

[8] Satoshi Ojika, Yushi Miura and Toshifumi Ise, "Inductive Contactless Power Transfer System with Coaxial Coreless Transformer for DC Power Distribution," *in Proceedings of IEEE ECCE2013* Asia Downunder (ECCE Asia), Melbourne, Australia, pp. 1046-1051, June 2013.

[9] Yusuke Hayashi, Hajime Toyoda, Toshifumi Ise and Akira Matsumoto, "Contactless DC Connector Based on GaN LLC Converter for Next-Generation Data Centers," *IEEE Trans. on Industry applications,* vol. 51, no. 4, pp. 3244-3253, July/August2015

[10] Yong Li, Ruikun Mai, Mingkai Yang, Zhengyou He, "Cascaded Multi-Level Inverter Based IPT Systems for High Power Applications," *Journal of Power Electronics*, vol. 15, no. 6, pp. 1508-1516, November 2015.

[11] Wenjin Sun, Hongfei Wu, Haibing Hu, Yan Xing, "Resonant Tank Design Considerations and Implementation of a LLC Resonant Converter with a Wide Battery Voltage Range," *Journal of Power Electronics*, vol. 15, no. 6, pp. 1446-1455, November 2015.

[12] Hong Huang, "Designing an LLC Resonant Half-Bridge Power Converter," 2010 Texas Instruments Power Supply Design Seminar, SEM1900, Topic 3, TI Literature Number: SLU.

[13] D. Graham Holmes, Thomas A. Lipo*, Pulse width modulation for power converter*: A John Wiley &Son, 2003, pp. 440-449.

[14] S. Khomfoi and L. M. Tolbert, Multi-level Power Converters, Power Electronics Handbook, 2nd Edition, Elsevier, Chapter 17, pp. 451-482. 2007.

Worapong Pairindra He was born in Thailand, in 1973. He received his B.Eng. degree in Electrical Engineering from Sripatum University, Bangkok, Thailand, in 1997, and his M.Eng. degree in Power electronics from the Assumption University, Bangkok, Thailand, in 2007. He is presently working toward his D.Eng. degree in Electrical Engineering at the King Mongkut's Institute of Technology Ladkrabang (KMITL), Bangkok, Thailand. His current research interests include power electronics application, multi-level converter and inductive power transfer system.

Surin Khomfoi He was born in Thailand. He received his B.Eng. and M.Eng. in Electrical Engineering from the King Mongkut's Institute of Technology Ladkrabang (KMITL), Bangkok, Thailand, in 1996 and 2000, respectively; and his Ph.D. degree in Electrical Engineering at the University of Tennessee, Knoxville, TN, USA, in 2007. Since December 1997, he has been a Lecturer with the Department of Electrical Engineering, KMITL, where he is currently presently an Associate Professor. His current research interests include multi-level power converters, renewable energy applications, fault diagnosis, power quality and smartgrids. Dr. Khomfoi is a Member of the Eta Kappa Nu Honor Society and a Senior Member of the IEEE. He was a recipient of academic scholarship awards, including full academic scholarship for his B.Eng., M.Eng., and Ph.D. studies from the Energy Policy and Planning Office (EPPO), Ministry of Energy Thailand.